A Channel Model for Multipath Interference On Terrestrial Line-of-Sight Digital Radio

Charles Henry Bianchi and Kondagunta Sivaprasad

***Abstract*— A comprehensive system model for characterizing the effects of multipath propagation on digital radio systems in the 4–6-GHz band is shown in this paper. The effects of terrain-induced multipath propagation in the presence of atmospheric anomalies are studied using data from experimental microwave links in the field and in the laboratory. This technique, which treats multipath propagation as digital signal distortions caused by interference from ground reflections, has not been shown previously. A forward multipath propagation model is used to identify the critical propagation parameters for a quadrature amplitude modulated (QAM) signal. A normalized two-ray channel model is developed to approximate the frequency response produced by interference from a ground reflection in a narrow band. The effectiveness of this channel model is evaluated using measured data from the test radio link in the laboratory and in the field.**

***Index Terms*—Interference, multipath channels.**

I. Introduction

THE radio channel on a microwave radio link is the free-space line-of-sight (LOS) path between the transmitting and receiving antennae. In the 6-GHz band, LOS path lengths vary from 5 to 95 miles. Propagation of electromagnetic waves with centimeter wavelengths may be approximated by geometrical optics techniques at these distances [1]. Signal loss is mainly due to spherical spreading of the wavefront.

Atmospheric anomalies lead to signal distortion. These are generally caused by variations in the index of refraction in the lower atmosphere. The lower atmosphere may be viewed as a lossy waveguide when the gradient of the index of refraction is nonlinear. A change in the gradient may cause defocusing or additional spreading of the wavefront. This results in additional attenuation of the signal. On the other hand, a change in the sign of the gradient may cause focusing or concentration of the wavefront. This results in signal superposition or surging. These phenomena are somewhat unusual and infrequent. Focusing is generally associated with atmospheric ducting, which requires very stable and enduring weather conditions. Atmospheric phenomena by themselves are not the dominant causes of impairment in digital radio systems and are not addressed in this study.

The earth is the lower boundary on a terrestrial microwave link. The transition in impedance from air to ground or air to water provides a reflection coefficient of near unity for the airborne signal. The likelihood of signal reflection from ground or water is very high. The fixed nature of the earth makes a stable reflection possible in the presence of stable weather conditions, giving rise to coherent interference. Coherent interference results in substantial impairment to a digital communication system. So there is a pressing need for the development of an appropriate channel model to analyze the performance of the digital modem.

Of the many techniques that have been used to study the radio propagation in the lower atmosphere, the most relevant are the diffraction models, refraction models, wave-equation models, and channel models. Diffraction models [2] compute the field strength as a function of position by computing equivalent fields at physical boundaries and obstacles. Refraction models [3] approximate the received wavefront as a function of position by integrating multipath rays. Wave models obtain the field strength as a function of position with computationally intensive wave equations. A lossy waveguide model suggests the evaluation of the waveguide equation [1]. A reflective ground model suggests the evaluation of the integral equation [4]. A surface-duct model suggests the evaluation of the parabolic equation [5]–[8]. Channel models use parameters [9]–[12] which may or may not be physical. The parameters are used to simulate the statistical behavior of the channel and thereby evaluate the performance of the digital communication link.

The purpose of this study is to develop a channel model for eventual integration into an overall digital system model. This characterization will provide a better understanding of the nature and likelihood of channel distortions due to multipath interference. In Section I, a two-ray channel model is developed for LOS microwave radio. In Section II, a forward multipath model is developed to predict multipath parameters from the link geometry. In Section III, the channel model is inverted to recover the two-ray parameters from signal measurements. A review of the techniques and results then follows.

II. Channel Model

Based on the nature of forward scattering on the terrestrial microwave link, a forward multipath model is developed for the radio channel. The received signal is approximated as the superposition of a direct signal and a second signal which is a reflected version of the direct signal. The model allows for simulation of a varying radio channel by selection of two-ray parameters.

Manuscript received March 3, 1997; revised January 7, 1998.

C. H. Bianchi is with the Sanders Lockheed-Martin Company, Nashua, NH.

K. Sivaprasad is with the Department of Electrical Engineering, University of New Hampshire, Durham, NH 03824 USA.

Publisher Item Identifier S 0018-926X(98)04621-3.

Phasors are used to approximate the vector addition of two interfering signals in a bandlimited channel. The two-ray channel response is composed of a direct signal $\underline{\alpha}$ and a secondary (delayed) signal $\underline{\beta}$. The channel response in the presence of multipath interference is then approximated as the vector sum of these two phasors. The resultant phasor has magnitude σ and phase ϕ that are functions of the signal and interference vectors $\underline{\alpha}$ and $\underline{\beta}$

$$\sigma e^{j\phi} = \alpha e^{j[2\pi f \tau_\alpha]} - \beta e^{j[2\pi f \tau_\beta]} \tag{1}$$

where τ_α is the propagation delay of the first ray and τ_β is that of the second. Normalizing the phase relationship to that of the direct ray results in a generalized representation for the composite signal

$$\sigma e^{j\phi'} = \alpha - \beta e^{j[2\pi f \tau']} \tag{2}$$

where the composite phase is

$$\phi' = \phi - j2\pi\tau_\alpha \tag{3a}$$

and the delay difference is

$$\tau' = \tau_\beta - \tau_\alpha. \tag{3b}$$

One of the causes of broad-band attenuation and delay distortion is multipath propagation. The result of multipath propagation is a superposition of two or more delayed replicas of the same transmitted signal at the receiver. If the delayed replicas are out-of-phase, the subsequent cancellation results in signal loss.

For given amplitudes and delays, the composite signal has been written as a function of frequency as in (1). However, for broad-band channels, signal cancellation is also a function of the delay difference as was discussed above. For signaling at a fixed bit rate (or in a fixed bandwidth), there are discrete delay differences (odd-integer half periods) yielding signal cancellation. If delay difference and frequency of cancellation are decoupled, the two phasor composite of (1) may be recast as a two-ray superposition. In a communication channel, having a bandwidth much narrower than the overall multipath channel, the delay difference is approximately constant with respect to frequency. By assuming a fixed delay difference as a function of frequency, the two-ray cancellation is expressed as a function of offset frequency from a given cancellation frequency. Independent selection of both delay and cancellation frequency are allowed with this model.

From (2), the generalized transfer function of the two-ray model normalized in frequency for a narrowband channel is

$$H(\Delta\omega) = \alpha - \beta e^{j[2\pi(f-f_0)\tau]}. \tag{4}$$

The parameter α, represents the strength of the direct signal. The parameter β represents the strength of the second path signal. The delay difference τ represents the delay of the second path signal with respect to the direct signal. The f_0 is the frequency of the signal cancellation. The expression $f - f_0$ represents the offset of the observation frequency from the frequency of the minimum signal power. The frequency of the signal power minimum is commonly referred to as the cancellation or "notch" frequency. It corresponds to the location of minimum signal power in the frequency domain. Strong second-ray interference results in substantial signal cancellation. Both the signal power loss at a frequency f (narrow band) due to f_0 and the distortion across the channel (broad band) due to τ cause impaired communication in the affected channel, as described earlier.

LOS microwave radio propagates in a half-space that is bounded by land or water. The energy reflected from the earth varies, depending upon the topology and the propagation characteristics of the lower atmosphere. Fluctuations in the refractivity of the lower atmosphere cause variations in the relative strength of the ground reflection β. The secondary delay τ or path length also varies.

The transfer function of the narrowband two-ray model in (4) may be expressed in terms of broad-band and narrow-band attenuation as

$$H(\Delta\omega) = a\left\{1 - be^{j[2\pi(f-f_0)\tau]}\right\} \tag{5}$$

where the parameter a represents the broad-band or "flat" attenuation and the parameter b represents the strength of the secondary signal normalized to the direct. When $f = f_0$, $H(\Delta\omega) = a(1-b)$, the minimum signal power.

In order to focus on the channel slope only, the transfer function of (5) may be scaled by the broad-band attenuation resulting in the normalized two-ray model,

$$H(\Delta\omega) = 1 - be^{j[2\pi(f-f_0)\tau]} \tag{6}$$

with the parameters as in (5). As before, the parameter b represents the strength of the secondary signal. In this case, the direct signal is the reference and the second signal is normalized to it. When $f = f_0$, $H(\Delta\omega) = (1-b)$, the minimum signal power (normalized).

There are two possible scenarios for dynamic multipath fading as modeled by two rays in this study. There may be a second signal of varying strength or a second path of varying delay.

For the case of varying second signal strength, b is allowed to change. However, the offset notch frequency $f - f_0$, broad-band attenuation a, and delay τ of the second signal with respect to the direct signal are fixed. The result is a changing notch depth. The process represents a propagation environment where there is a boundary that is stable in position as a function of the propagation wavelength. However, the reflected energy is not stable in strength. A stable refractive index gradient in the lower atmosphere will give rise to a constant secondary path delay. A discontinuity or abrupt change in the refractive index gradient at some fixed altitude may give rise to refracted rays. An example would be the formation of a homogeneous layer in the lower atmosphere. Such a layer would be transient in nature and vary in height and density. On the other hand, the formation of a coherent reflecting area on exposed ground is a much more predominant and stable source of reflected energy. As the ground becomes more coherent in its reflectivity, there is an increased reflection coefficient. The result is a stronger secondary ray. Changes in the effective bending of rays within the lower atmosphere may cause focusing or defocusing effects. The result is a modulation of the secondary ray strength.

For the case of the second path of varying delay, the reflection phase is allowed to change. The result of phase or delay change is a variation of the exponental term $\tau(f - f_0)$. In reality, the secondary ray delay τ is varying. However, the phase change is also reflected in variation of the minimum signal power frequency f_0. The relative change in delay is very small and so it is treated as a constant. A boundary having a stable reflectance amplitude but an unstable position as a function of the propagation wavelength would cause notch movement. Nonstable path length is very likely a result of a changing refractive index gradient in the lower atmosphere. This effect modulates the path length of a signal reflected from the ground.

In general, with minimum phase an increasing notch frequency is equivalent to a widening notch separation. This corresponds to a decreasing delay difference. In a minimum phase two-ray channel the dominant path arrives at the receiver first. With minimum phase, an increasing notch frequency is equivalent to a positive delay difference, which is decreasing in magnitude. On the other hand, in a nonminimum phase two-ray channel, the dominant path arrives at the receiver later. With nonminimum phase, an increasing notch frequency is equivalent to a negative delay difference, which is decreasing in magnitude. The direction of change in delay for nonminimum phase (less negative) is opposite to the direction of change for a minimum phase (less positive). An ambiguity exists in the relationship of delay difference and notch separation. A minimum phase fade with increasing notch frequency has a second path delay gradient that is similar to that of a nonminimum phase fade with decreasing notch frequency.

III. Forward Multipath Model

In this section, a forward multipath model is developed by examining transmission of the signal from the source over the air to the receiver. The terrain is treated as a piecewise linear scatterer that may give rise to many reflected signals at the receiver and interfere with the direct signal, as described in Section I. The lower atmosphere variations are expressed as changes in the gradient of the index of refraction. They are treated as displacement of the propagation paths for the direct and reflected rays. The principles of geometrical optics are used to compute reflected rays. The reflecting areas of ground and their respective parameters are identified by simulation. These are compared to measured data from an experimental microwave link.

In order to determine the parameters of the reflected signals, the conditions of propagation in the lower atmosphere must be included.

In the lower atmosphere, the radio refractivity N is defined by /

$$N = (n - 1) \cdot 1E - 6 \tag{7}$$

where n is the index of refraction of the atmosphere. For a constant refractivity index, the path of the ray is a circle of radius R where

$$1/R = dN/dh \cdot 1E - 6 \tag{8}$$

and h is the height above the earth [13].

A transformation of variables allows a change of perspective from curved earth to flat earth. A ray of radius R propagating above the earth has a modified radius Rm above the flat earth

$$1/Rm = 1/R + 1/a \tag{9}$$

where $a = 6370$ km (earth radius). For a constant refractivity index, the path of the ray is a circle of radius Rm where

$$1/Rm = dM/dh \cdot 1E - 6 \tag{10}$$

where M is the modified radio refractivity for flat earth propagation related to N by

$$M = N + (h/a) \cdot 1E - 6. \tag{11}$$

The ratio of modified to actual earth radius is defined as the effective earth radius factor

$$K = Rm/a. \tag{12}$$

Normal daytime propagation conditions in the lower atmosphere exist when $K = 4/3$ or $dN/dh = -39$ N units/km. A small negative gradient in the refractivity of the atmosphere causes the radio waves to follow the curvature of the earth.

Subrefractive propagation occurs when dN/dh is greater than -39 N units/km and less than infinity. In this case, K is greater than 0.5 and less than 4/3. It causes an upward bending of rays or an apparent bulge in the earth surface. Power fading results from the additional spreading of the wavefront. Diffraction losses result in cases of obstruction fading from earth bulge.

Super-refractive propagation occurs when dN/dh is less than -39 N units/km and greater than -157. In this case K is greater than 4/3 and less than infinity. The earth appears to be flat or concave, causing rays to hit the earth before arriving at the receiver. Power fading results from the additional spreading of the wavefront. Multipath interference results in cases of increased or enhanced ground reflections.

Variations in K on a microwave link are caused by changes in the index of refraction as a function of altitude. The index of refraction is composed of dry and wet components, N_{dry} and N_{wet} [14]. The composite is a function of pressure, humidity, and temperature. The dry component increases in value with both temperature and humidity, as is shown in Fig. 1(a). The wet component increases with saturated vapor pressure, as is shown in Fig. 1(b).

In the modeling of radio propagation for LOS microwave radio, the gradient of the index of refraction is commonly assumed to be linear in the lower atmosphere (100 m) and constant along the microwave link [1], [14], [15]. As a result, the K factor of (12) is used for the ratio of the radius of propagation of radio waves above the earth to the actual radius of the earth. Equations (7)–(12) illustrate the relationship between the index of refraction and the K factor. As the gradient of the index of refraction becomes less positive, the K factor increases. When the gradient becomes negative, the K factor exceeds one. This is shown in Fig. 1(c).

This paper is concerned with terrain-induced multipath interference. This is possible and probable in a link with exposed and reflective areas of ground under typical and stable atmospheric conditions. In such cases, the lower atmosphere

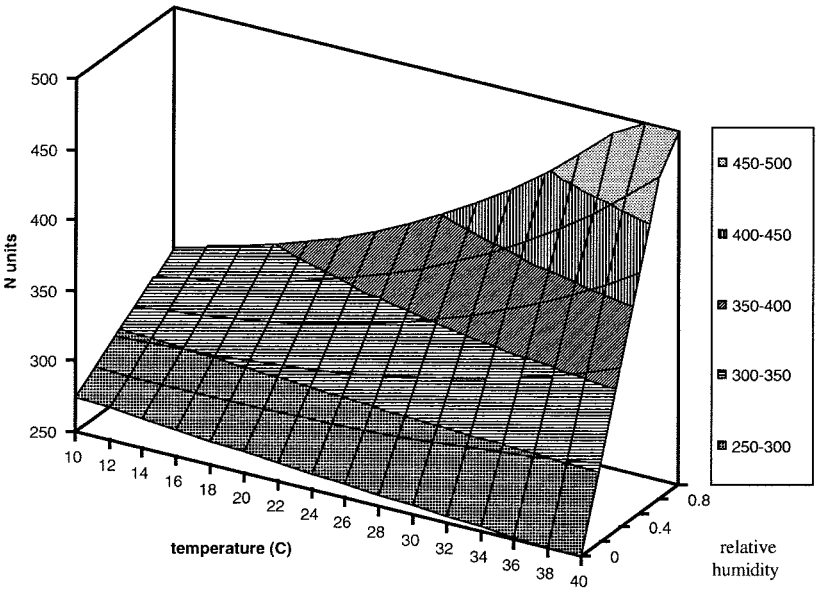

(a)

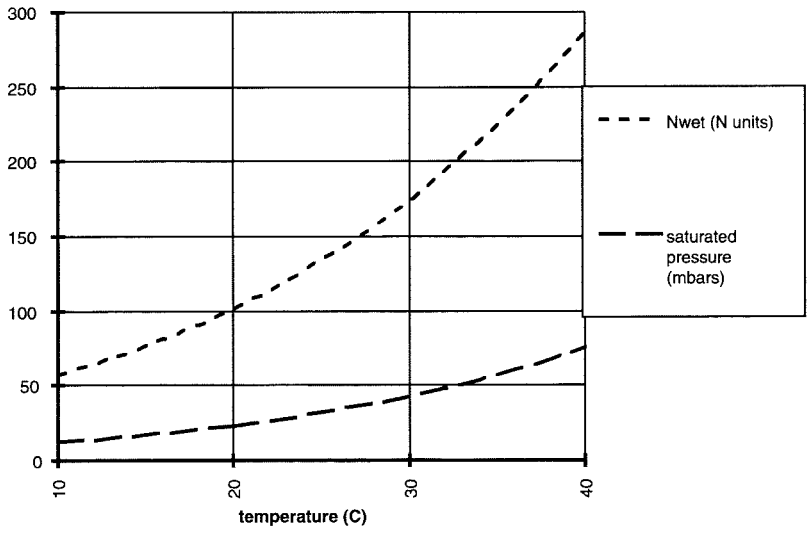

(b)

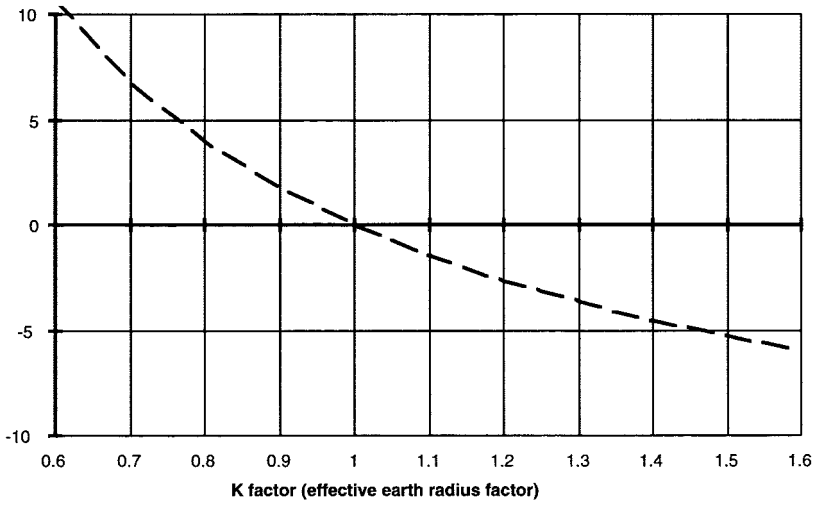

(c)

Fig. 1. (a) Index of refraction ($N_{\rm dry}$). (b) Index of refraction ($N_{\rm wet}$) and saturated pressure (es). (c) Gradient of the index of refraction in the lower atmosphere (100 m) as a function of a constant K.

is homogeneous and well-mixed throughout the link. The K factor is used to model the typically linear variations in the refractive index gradient as a function of altitude. It is constant with respect to distance under these conditions.

A method for path-profile linearization is developed to identify potentially coherent reflecting areas as well as areas of shadowing and possible obstruction. Terrain elevation points are adjusted to account for the effective change in path length. The adjusted linearized profile is treated as a combination of reflecting plates and wedges from which a reflected ray is computed. The effects of directive antenna data are included to allow for simulation of real radio systems.

The coordinate system is Cartesian. The origin is at sea level under the first antenna. The horizontal axis is to sea level under the second antenna. The earth bulges upward above the horizontal axis.

The terrain-elevation profile is plotted for a flat earth. LOS propagation is along the direct optical path (straight line) from the transmitting to the receiving antenna. For the flat-earth profile, the direct path is fixed. In the absence of atmospheric refraction, the direct path is perpendicular to the radius of the earth and the optical (apparent) and physical (actual) terrain locations are equal. Atmospheric refraction bends the propagation paths of the radio waves (e.g., earth bulge). The result is a displacement of the optical terrain location. Thus, for the flat-earth profile the optical-terrain elevation varies as a function of atmospheric refraction.

Secondary rays will be delayed according to the length of the propagation path. The path of the secondary ray is defined as the sum of straight line segments (hypotenuse) from antenna to ground segment to antenna.

Reflecting segments are assigned an altitude above sea level, which includes earth bulge effects. The terrain-elevation data are mapped to a flat-earth profile. The distance from each reflecting segment to an antenna is measured horizontally. The path length is a straight-line segment from the transmitting antenna to the reflection point and from the reflection point to the receiving antenna.

The propagation paths are straight lines in Cartesian coordinates. Subrefraction and super-refraction are treated as parabolic distortions of the local terrain altitude above sea level. The terrain-elevation data are entered as a series of elevations along the path of transmission. These elevations are displaced for the desired gradient of the index of refraction (or K factor) by computation of the modified earth radius. A front-end subroutine then computes a series of straight-line segments of 0.01 miles in length to approximate the profile. The slope of the segment is defined by the difference in elevation of the endpoints after accounting for earth bulge condition.

Each segment may be shadowed or obstructed from view of either antenna by the surrounding terrain. The first pass of the analysis is a clearance profile. Illumination conditions of the local ground are determined by sweeping the profile from each end. A monotonic decrease of the angle of arrival at the ground segment from one antenna compared to the angle of departure from the ground segment to the other antenna implies a nonshadowed condition. Visibility is the first parameter of the forward multipath model.

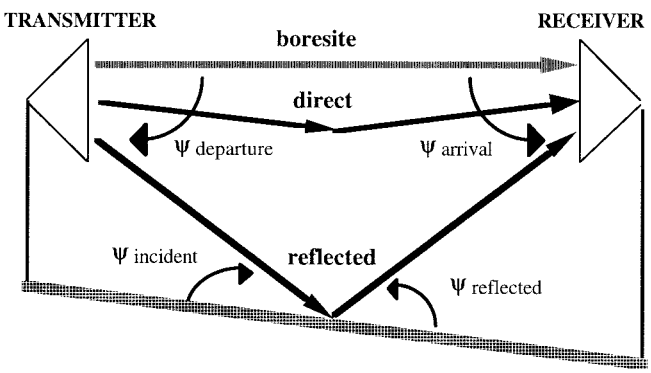

Fig. 2. Local geometry of ground reflection.

For worst-case analysis, each exposed ground segment is considered a reflecting surface having a reflection coefficient equal to unity. In fact, for grazing angles of incidence, the reflection coefficient of ground is very close to unity for microwave radio frequencies and for both vertical and horizontal polarizations [15]. This reflection coefficient is the second parameter of the forward multipath model.

The amplitude of the signal is reduced by the distance from the source squared because of the spherical propagation of a wavefront in free-space. The direct signal strength is therefore attenuated by the path length traveled from the transmit to the receive antennas. The secondary signal travels a different path and is attenuated by a different amount. For the purposes of this model, the direct signal amplitude is normalized to unity and the secondary signal amplitude is scaled by the difference in path length squared. Thus, the third parameter for the forward multipath model is signal amplitude.

The launched and detected signals are also scaled by an approximate antenna pattern with the peak aligned with boresite and normalized to unity. The direct signal strength is, therefore, attenuated by the transmit and receive antenna patterns. The antenna contribution is simply a function of the departure and arrival angles. On the other hand, the secondary path is attenuated by the transmit and receive antennas and by the directivity of the reflecting surface. Assuming the exposed earth to be a near-perfect reflector, Snell's law is applied for ray tracing. However, the path from the transmitter to the reflecting ground segment and the path from that same ground to the receiver may not have equal arrival and departure angles. In other words, the receiver may be off boresite for the reflection path. Since each ground segment provides an aperture for an image source, the reflection is treated as a windowed image of the actual source. As with the direct path, the reflection path is scaled by an approximate antenna pattern with the peak signal at boresite normalized to unity. For the secondary path, the antenna contribution is a function of the departure, incidence, reflection, and arrival angles. Thus, the fourth parameter for the forward multipath model is directivity. The reflection geometry for a second (ground reflection) path is illustrated in Fig. 2.

Also important to the reflection criterion is the smoothness of the reflecting surface. If the ground segment is rough with respect to the wavelength of propagation, the reflection will be scattered or diffuse. If it is smooth with respect to the

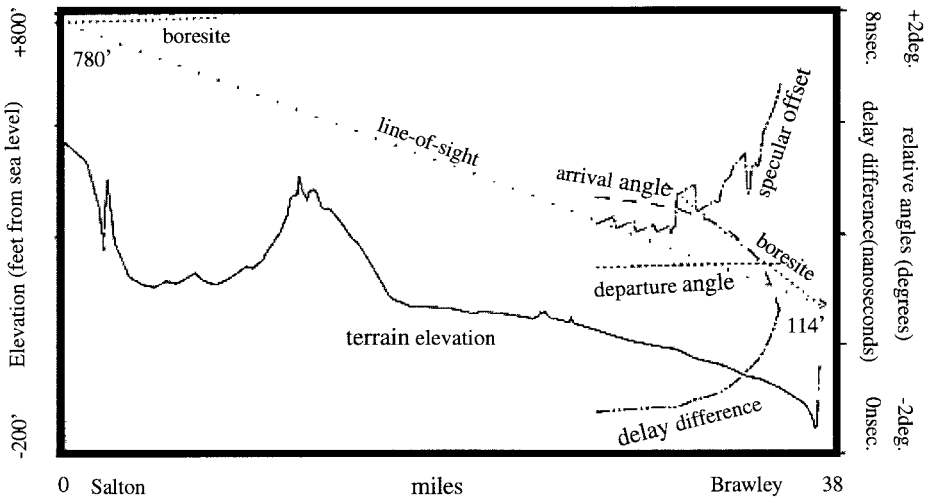

Fig. 3. Forward multipath model ($f = 6$ GHz, $K = 2/3$).

wavelength of propagation, the reflection will be mirror-like or specular. As a rule, the Rayleigh criterion [13], [14] is used to distinguish smooth from rough surfaces. The difference in path length Δl may be written as a function of the variation in local surface height h and the angle of incidence on the local surface area α

$$\Delta l = 2h \sin \alpha. \tag{13}$$

In general, any surface for which the path lengths of reflected rays vary by much less than a wavelength λ

$$h(\sin \alpha)/\lambda \to 0$$

is considered smooth. A microscopic smoothness criterion of $\pi/4$ or

$$\Delta l < \lambda/8 \tag{14}$$

applied over an individual ground segment results in a surface height difference limit of

$$\Delta h < \lambda/16(\sin \alpha).$$

If $\lambda = 0.05$ m, $\alpha = 0.05°$ then $\Delta h < 0.0625$ m. The roughness of a ground segment is the fifth parameter for the forward multipath model.

Similarly, the macroscopic smoothness of several consecutive segments is an important factor in determining the convergent nature of the reflecting area. If several adjacent segments satisfy a criterion such as (14), then they are merged into a larger area of specular reflection. The rays reflected from such an area are all in phase, giving rise to a continuous and contiguous reflected wavefront. For digital radio, the resulting interference will be coherent and signal like. The stability of superposition will be a function of the stability of the propagation path, composed of the reflecting ground or water and the lower atmosphere. The addition of multiple signals at the receiver will result in summation and cancellation that is a function of the delay difference of the propagation paths. If the abovementioned criterion are exceeded, then the overall area will act as a diffuse reflector. The resulting interference from this type of reflection will be noncoherent and noise like. In the channel of concern, it will be weak because the noise is broad band. The result will be a slight increase in the random noise power. The convergence of adjacent ground segments or the resulting coherence of the reflected wavefront is thus a sixth parameter for the forward multipath model.

In summary, second path clearance and reflector smoothness are necessary for a reflected signal to be generated. If a surface area is illuminated and sufficiently smooth, it will serve as a reflector for a secondary path. However, coherence is the most important parameter for interference to occur once the path is established. If the reflected wavefront is coherent, then the reflected signal will interfere with the direct coherent signal. The interference will result in channel distortion and loss of performance. Because of the threshold effect of digital decisions, variations in reflection coefficient or antenna descrimination will not affect the loss of performance. They only affect the amount of signal attenuation at the cancellation frequency. In fact, it is more important to properly characterize the second path delay, as adjacent surfaces that create constant delay paths form a coherent wavefront.

Forward multipath results for the Salton to Brawley link in southern California are tabulated in Table I and illustrated in Figs. 3 and 4. The LOS path is indicated by the coarse dotted line and the boresight direction of the antennas (aligned at $K = 4/3$) is indicated by the fine dotted line. The LOS path is 37 miles in length. The path parameters are: 1) terrain elevation; 2) angle of departure (from the transmitter); 3) angle of arrival (at the receiver); 4) angle from specular (at the reflecting surface segment); and 5) delay (of the reflection path relative to the LOS path). The terrain elevation 1) is plotted for each surface segment with a solid line. The remaining parameters are computed and then superimposed onto the terrain elevation profile if the respective ground segment is in sight of the transmitter and receiver. The angle of departure 2) is indicated by a fine dashed line. The angle of arrival 3) is indicated by a coarse dashed line. The angle from specular 4) is indicated by a solid line broken by one dash. The delay 5) is indicated by a solid line broken by two dashes. Terrain that gives rise to coherent reflection is indicated by a convergence of constant delay and constant angle-from-specular profiles.

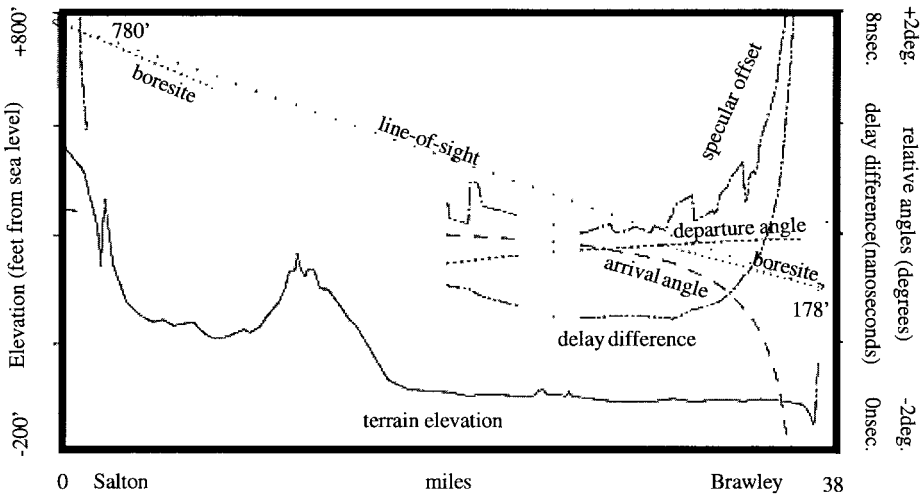

Fig. 4. Forward multipath Model ($f = 6$ GHz, $K = 5/3$).

TABLE I
FORWARD MULTIPATH RESULTS

K factor	Receiver Antenna (elevation in feet)	Second Path (delay in nanoseconds)
2/3	141	.8
1	141	1.2
4/3	141	1.6
5/3	141	2.2
2/3	178	1
1	178	1.6
4/3	178	2.0
5/3	178	2.4

The path analysis for $K = 2/3$ is plotted in Fig. 3. The terrain slopes downward from Salton to Brawley, with a significant hill providing some blockage at approximately one third of the distance from Salton to Brawley. The direct signal path is not obstructed. Note that the antenna alignment for the transmitter and receiver is normally performed during standard propagation conditions ($K = 4/3$). As a result, the LOS for $K = 2/3$ is below the LOS for $K = 4/3$. Therefore, the direct signal for $K = 2/3$ is attenuated by the antenna gain offset from the maximum gain direction at $K = 4/3$. The multipath parameters are plotted for the sections of the length, which are visible to both the transmitter and receiver. This occurs along the last third of the distance from Salton to Brawley. In this area, the angles of departure and arrival are small and nearly equal, indicating that the effect of antenna discrimination is insignificant. Furthermore, the angle from specular is nearly zero over the first half of the reflecting area indicating angles of incidence and reflection from the ground that are equal. The reflection is specular and mirror like and the delay is nearly constant and approximately equal to 0.8 ns over the first half of the reflecting area. Therefore, an interfering signal is possible due to a coherent wavefront with an 0.8-ns delay reflected from the first half of the last third of the distance from Salton to Brawley.

The path analysis of Fig. 3 was performed for a Salton antenna height of 780 ft and a Brawley antenna height of 141 ft and a $K = 2/3$. Over approximately 10% of the path near Brawley, the angle of reflection from specular is very close to 0°. Over the same area, the delay is approximately 0.8 ns, indicating a possibly coherent reflection source. Additional analyses were performed with different K (Table I, rows 1–4). For $K = 1$ the delay is slightly increased to 1.2 ns, as would be expected with the increased gradient in index of refraction. The angle from specular is approximately zero for the reflected wavefront directed at the receiver. At $K = 4/3$ the delay is again slightly greater at 1.6 ns with a very nearly specular reflection angle. In this case, a second reflecting area becomes exposed adding approximately 5% to the path length. For $K = 5/3$ the delay increases to 2.2 ns with a near specular reflection. Here, the original reflecting area has grown in size to approximately 15% of the path length; also, a second reflecting area is exposed, giving rise to a third propagation path. Throughout the propagation regime of Fig. 3, the simulation shows evidence of probable interference from ground reflections. Furthermore, the variation in delay of the reflection path would suggest a distribution of cancellation frequencies, or, in other words, broad-band cancellation effects.

Additional path analyses were performed for various K with a Salton antenna height of 780 ft and a Brawley antenna height of 178 ft (Fig. 4, Table I, rows 5–8). Over approximately 10% of the path near Brawley the angle of reflection from specular is close to 0° for $K = 2/3$. As before, the delay is approximately 1 ns over the same area. With $K = 1$ the delay increases to 1.6 ns, as would be expected with the increased height and gradient in index of refraction. The angle from specular is again approximately zero directed at the receiver. At $K = 4/3$, the delay increases again to 2.0 ns, with a very nearly specular reflection angle. A second reflecting area is

again exposed, comprising an additional 5% of the path and giving rise to a possible third propagation path. For $K = 5/3$ (shown in Fig. 4), the delay increases to 2.4 ns with a near specular reflection. Here, the original reflecting area has grown in size to approximately 15% of the path length and the second reflecting area remains exposed. As in Fig. 3, the propagation regime of Fig. 4 shows evidence of probable interference from ground reflections. The change in antenna height does not diverge or defocus the reflected energy. It serves only to alter the delay of the reflected paths.

IV. Inverse Multipath Model

In order to determine the parameters of the forward multipath model, the characteristics must be compared to the observable behavior of the radio channel. In this section, an inverse multipath model is developed. The inverse model allows for estimation of the channel transfer function developed in Section I. A direct signal and an interfering signal are approximated at the receiver. While the parameters of the model are not easily measured, they must be recoverable from the channel data in order for the model to successfully approximate the channel. To recover the parameters, the two-ray cancellation model of Section I is inverted. The model is set equal to the channel power, and solutions for the various parameters are obtained in terms of measured levels. Recovery of the parameters is equivalent to identification of the interference for cases of good channel approximation, as is shown.

Linear and parabolic power distortions of the channel transfer function are characterized using a second order approximation

$$|H(f_n)|^2 = p_0 + p_1 f_n + p_2 f_n^2 \tag{15}$$

where p_0, p_1, and p_2 represent the zero order (constant), first order (linear), and second order (parabolic) coefficients of the power of the channel transfer function. The normalized frequency f_n is the ratio of frequency to channel bandwidth.

The coefficients may be determined using a least-mean squares parabolic regression technique. The data points are the received signal power values measured by the three channel filters at the frequencies f_1, f_2, and f_3, respectively. The least-mean squares technique minimizes the difference between the second-order polynomial and the data points. The coefficients are computed by solving the system of equations

$$\begin{bmatrix} 1 & f_1 & f_1^2 \\ 1 & f_2 & f_2^2 \\ 1 & f_3 & f_3^2 \end{bmatrix} \begin{bmatrix} p_0 \\ p_1 \\ p_2 \end{bmatrix} = \begin{bmatrix} |H(f_1)|^2 \\ |H(f_2)|^2 \\ |H(f_3)|^2 \end{bmatrix}. \tag{16}$$

Solutions were restricted to cases having a cancellation frequency falling inside the digital radio channel bandwidth. For such situations, there was only one solution to the system and it was not necessary to evaluate the stability of the equations.

The two-ray approach may be used to simulate the shape of the radio channel. The dispersive part of multipath fading may be simulated using a normalized two-ray model as in Section I, having the transfer function

$$H(\Delta\omega) = 1 - b\, e^{j[2\pi(f-f_0)\tau]}. \tag{17}$$

The offset cancellation frequency $f - f_0$ is the frequency relative to the position of the signal-power minimum. The parameter b represents strength of the second ray and the τ represents the delay difference of the second ray with respect to the direct ray.

The power in the channel and subsequent derivatives are expressed in terms of the magnitude squared

$$|H(\Delta\omega)|^2 = 1 - 2\,b\,\cos[\Delta\omega\tau] + b^2 \tag{18a}$$

$$\frac{\partial}{\partial(\Delta\omega)}\,|H(\Delta\omega)|^2 = 2\,b\tau\,\sin[\Delta\omega\tau] \tag{18b}$$

$$\frac{\partial^2}{\partial(\Delta\omega)^2}\,|H(\Delta\omega)|^2 = 2\,b\tau^2\,\cos[\Delta\omega\tau] \tag{18c}$$

where

$$\Delta\omega = 2\pi(f - f_0).$$

As the cancellation frequency approaches the frequency of observation, the offset cancellation frequency approaches zero and the first and second derivatives of (18a)–(18c) may be written as follows:

$$\frac{\partial}{\partial\Delta\omega}\,|H(\Delta\omega)|^2 = 2b\tau(\Delta\omega\tau) \tag{19}$$

and

$$\frac{\partial^2}{\partial\Delta\omega^2}\,|H(\Delta\omega)|^2 = 2b\tau^2 \tag{20}$$

for

$$(\Delta\omega) \Rightarrow 0.$$

The derivatives (19) and (20) may be used to estimate the offset cancellation frequency $\Delta\omega$ from which f_0 may be obtained at the channel center ($f = 0$)

$$(\Delta\omega) = \left[\frac{\partial}{\partial\Delta\omega}\,|H(\Delta\omega)|^2\right] \Big/ \left[\frac{\partial^2}{\partial\Delta\omega^2}\,|H(\Delta\omega)|^2\right]. \tag{21}$$

Furthermore, the channel power may be approximated by a parabola determined from the measured power at three frequencies within a narrow-band channel. The minimum power may be estimated from the channel power and its first two derivatives as evaluated at the channel center and the second ray strength may be calculated, as shown in (22) at the bottom of the next page. The second derivative (20) and the second ray strength (22) may then be used to estimate the second ray delay

$$\tau = \left\{\left[\frac{\partial^2}{\partial\Delta\omega^2}\,|H(\Delta\omega)|^2\right] \Big/ [2b]\right\}. \tag{23}$$

Given a parabolic approximation to channel power as shown earlier, it is possible to estimate the two-ray model parameters specified above. The polynomial in (15) is an expansion about the channel center frequency. Three coefficients, p_0, p_1, and p_2, are specified. The coefficients are related to the polynomial

and its first and second derivatives at the reference frequency as follows:

$$|H(0)|^2 = p_0 \tag{24}$$

$$\frac{\partial}{\partial f_n}|H(0)|^2 = p_1 \tag{25}$$

and

$$\frac{\partial^2}{\partial f_n^2}|H(0)|^2 = 2p_2. \tag{26}$$

The two-ray equation in (18a)–(18c) is a broad-band expression for power. Near the notch, the three parameters $(f - f_0)$, (b), and (τ) may be approximated by (21)–(23). As the notch frequency nears the channel center, the polynomial approximation and the two-ray model become comparable in validity. The two-ray parameters may then be estimated directly from the polynomial coefficients. The offset notch frequency becomes

$$f_0 = -[p_1]/[2p_2] \tag{27}$$

the second ray strength becomes

$$b = 1 - \sqrt{p_0 - \tfrac{1}{2}\{[p_1]^2/[2p_2]\}} \tag{28}$$

and the second ray delay becomes

$$\tau = \{[2p_2]/[2p_2]\}. \tag{29}$$

Physical measurements of multipath fading parameters and their variations have been well documented. Data have been published both internally to AT&T Bell Laboratories and in several references [16]–[18]. Various notch-frequency speeds, some as fast as 100 MHz per second have been recorded. Notch-depth speeds on the order of tens of decibels per second have also been noted.

Multipath transit delay data has also been published in several references. The data has varied widely. One reference gave a delay distribution with values less than 1 ns for 95% of the measured time [18]. Another published specific delays of 5–8 ns for atmospheric events [19]. In terms of path length, Crawford and Jakes [20] measured changes from fractions of 1–10 ft. The corresponding variations in angle of arrival were 0.75° above boresight to 0.8° below.

A typical multipath event from Brawley, CA, recorded for 6-GHz radio is shown in Fig. 5. The three spectrum filters separated by ±11 MHz from the channel center are monitored. The sampling rate is approximately eight times per second. An 11 s channel distortion event is shown at the two receiving antennas: Fig. 5(a) for the unprotected antenna and Fig. 5(b) for the space-diversity antenna. During both measurements, there was a notch moving through the band from high to low

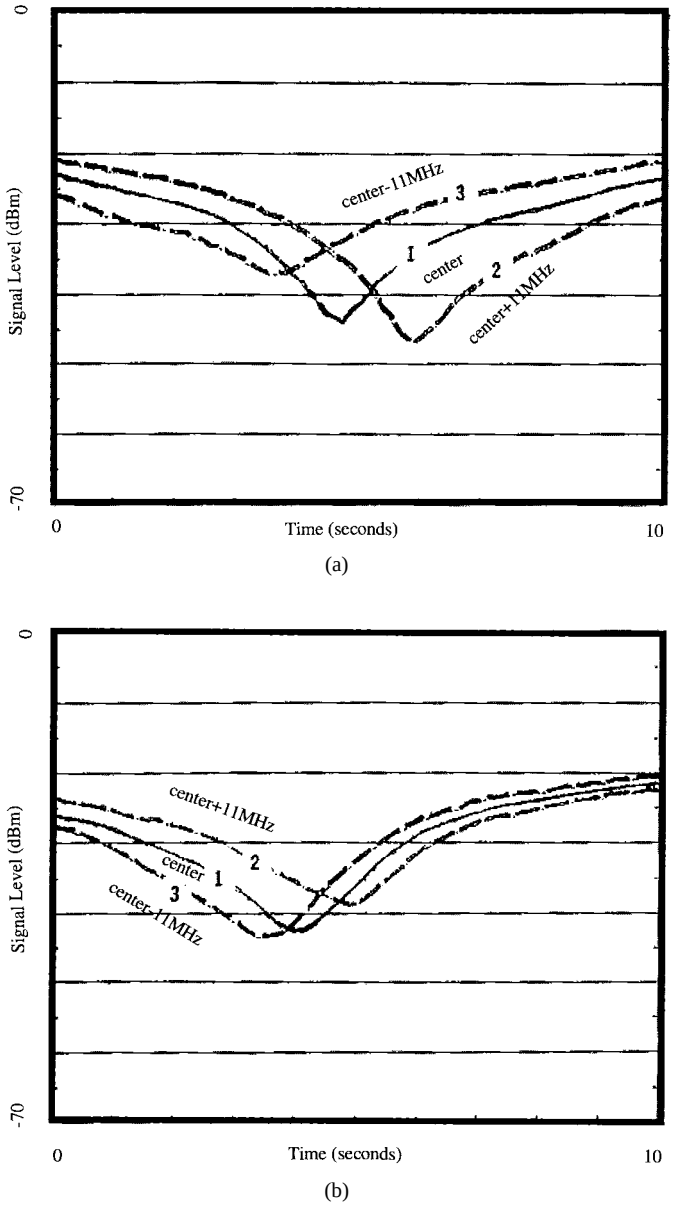

Fig. 5. (a) Measured multipath event (178 ft, 6 GHz—Brawley, CA). (b) Measured multipath event (141 ft, 6 GHz—Brawley, CA).

frequencies. This was shown by the gradual loss of signal in consecutive filters.

In a two-ray fading scenario, the transfer function in the frequency domain may be viewed as a notch filter with varying position and magnitude of the notch or minimum. The channel distortions associated with an unstable minimum are traumatic to digital signaling. In a nonhomogeneous atmosphere, slight variations in wind speed, temperature, pressure, and humidity may occur simultaneously, resulting in both a phase and amplitude modulation of the received signals. Changes in relative

$$b = 1 - \sqrt{|H(\Delta\omega)|^2 - \frac{1}{2}\left\{\left[\frac{\partial}{\partial\Delta\omega}|H(\Delta\omega)|^2\right]^2 \Big/ \left[\frac{\partial^2}{\partial\Delta\omega^2}|H(\Delta\omega)|^2\right]^2\right\}} \tag{22}$$

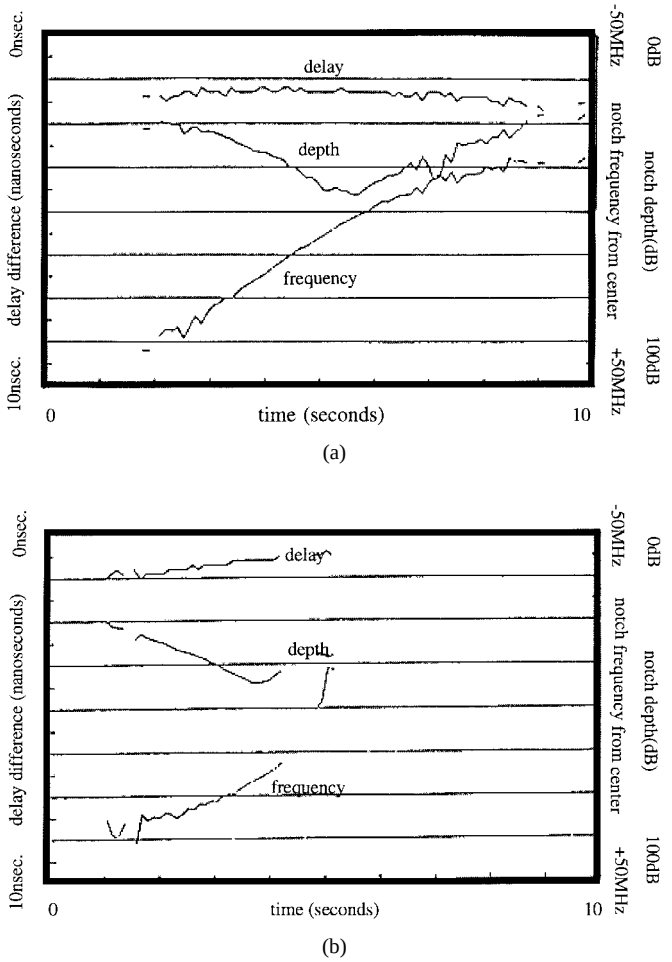

Fig. 6. (a) Inverted multipath model (178 feet, 6 GHz—Brawley, CA). (b) Inverted multipath model (141 feet, 6 GHz—Brawley, CA).

phase between two received signals results in a movement of the cancellation frequency or notch. Changes in amplitude result in a variation of the notch depth. Slope fading generally occurs when the notch is outside the monitored channel, but near the band edge. It is manifested by nonequal signal levels from each of the filters at the same instant in time, typically, with the band centered filter output being less than one band-edge filter output and greater than the other. As the signal minimum approaches a channel in the frequency domain, the slope of the channel response becomes more severe. The band-edge filter near the notch displays a large loss of signal. Eventually, the channel shape as given by the three filter outputs becomes nonlinear in decibels.

A good example of multipath propagation phenomenon is shown in Fig. 5(a) and (b). Initially, in the spaced antenna channel and then in the unprotected antenna channel, the signal power was faded and distorted. The spectra in Fig. 5(a) and (b) had a slope distortion as shown by the lower signal level in the upper filter output (f_3) and the higher signal level in the lower filter output (f_1). Movement of a signal minimum through a monitored channel is typically illustrated by the consecutive depression of each of the spectrum filter outputs in either ascending or descending order with respect to time as the notch sweeps to either higher or lower frequencies. A minimum rapidly moved from higher frequencies down through the spaced antenna channel. Seconds later, a minimum moved similarly through the unprotected antenna channel. A signal minimum in the frequency domain is a severe shape distortion of the channel causing quadrature crosstalk and loss of information.

The event was analyzed using the polynomial approximation to the normalized two-ray model. This determined delay, depth, and frequency of the fade. As is shown in Fig. 6(a) and (b), the normalized two-ray model is solved for both the unprotected and space-diversity ports. The analysis reveals minima moving approximately 15 MHz/s. At the unprotected antenna port, the second ray delay is approximately 2 ns for the duration of the event. Similarly, it is approximately 1 ns at the space-diversity port. The stability of the second ray delay is an important result of this analysis since it verifies the existence and dominance of the coherent interference signal. In general, the delays computed for this event fall within the range of the values published for other experiments (1–8 ns) [16]–[18].

V. Summary

The parameters for multipath propagation due to ground reflections are: 1) amplitude of the transmitted signal; 2) visibility of the exposed ground; 3) reflection coefficient of the exposed ground; 4) roughness of the exposed ground; 5) directivity gain for the path trajectory; and 6) coherence of the reflected wavefront. As is shown in the path analyses, it is essential to identify and analyze the sources of secondary paths. Visibility and directivity are easily established by a linearized terrain profile analysis. Coherence may be determined from the secondary path length or delay profile. A measurable area of exposed and smooth ground or water having a constant delay profile is a reflection candidate. If the coherent reflecting area is present for normal K factors, then the link has a large probability of multipath interference. On the other hand, if the coherent reflecting area is present for extreme K factors only, then the probability of multipath interference is small.

References

[1] A. J. Giger, *Low-Angle Microwave Propagation, Physics, and Modeling.* Norwood, MA: Artech House, 1991.
[2] K. Chamberlin and R. Luebbers, "Evaluating Longley–Rice and GTD propagation models," *IEEE Trans. Antennas Propagat.*, vol. AP-30, p. 1098, Nov. 1982.
[3] I. P. Shkarofsky and S. B. Nickerson, "Computer modeling of multipath propagation: Review of ray-tracing techniques," *Radio Sci.*, vol. 17, no. 5, p. 1133, Sept./Oct. 1982.
[4] J. T. Hviid, J. B. Andersen, J. Toftgard, and J. Bojer, "Terrain-based propagation model for rural area—An integral equation approach," *IEEE Trans. Antennas Propagat.*, vol. 43, pp. 41–46, Jan. 1995.
[5] M F. Levy, "Parabolic equation modeling of propagation over irregular terrain," *Electron. Lett.*, vol. 26, no. 15, pp. 1153–1155, Apr. 1990.
[6] ——, "Horizontal parabolic equation solution of radiowave propagation problems on large domains," *IEEE Trans. Antennas Propagat.*, vol. 43, pp. 137–144, Feb. 1995.
[7] S. W. Marcus, "A hybrid (finite difference-surface Green's function) method for computing transmission losses in an inhomogeneous atmosphere over irregular terrain," *IEEE Trans. Antennas Propagat.* vol. 40, pp. 1451–1458, Dec. 1992.
[8] A. Barrios, "A terrain arabolic equation model for propagation in the troposphere," *IEEE Trans. Antennas Propagat.* vol. 42, pp. 90–98, Jan. 1994.

[9] J. Lavergnat and M. Sylvain, "Selective fading radio channels: Modeling and prediction," *IEEE J. Select. Areas Commun.*, vol. SAC-5, pp. 378–388, Apr. 1987.
[10] M. Shafi, "Statistical analysis/simulation of a three ray model for multipath fading with application to outage prediction," *IEEE J. Select. Areas Commun.*, vol. SAC-5, pp. 389–401, Apr. 1987.
[11] E. H. Lin and A. J. Giger, "Radio channel characterization by three tones," *IEEE J. Select. Areas Commun.*, vol. SAC-5, pp. 402–415, Apr. 1987.
[12] J. Lavergnat and P. Gole', "Statistical behavior of a simulated microwave multipath channel," *IEEE Trans. Antennas Propagat.*, vol. 39, pp. 1699–1706, Dec. 1991.
[13] D. E. Kerr, *Propagation of Short Radio Waves.* New York: Dover, 1967, p. 411.
[14] M. P. M. Hall, *Effects of the Troposphere on Radio Communication.* Stevenage, U.K.: Peregrinus, 1979, p. 86.
[15] L. Boithias, *Radiowave Propagation.* New York: McGraw-Hill, 1987, p. 55.
[16] A. J. Bundrock and J. V. Murphy, "A broad-band 11-GHz radio propagation experiment," *IEEE Trans. Antennas Propagat.*, vol. AP-32, pp. 449–455, May 1984.
[17] L. Martin, "Rates of change of propagation medium transfer function during selective fading," in *URSI-F Symp.*, Louvain, Belgium, June 1983, p. 31.
[18] M. Rooryck, "Validity of two-path model for calculating quality of digital radio links; determination of model from measurements on analogue links," *Electron. Lett.*, vol. 15, no. 24, pp. 783–784, Nov. 1979.
[19] R. W. Hubbard and T. J. Riley, "Summary of propagation conditions and digital radio performance across the English Channel," in *ICC'89*, Sept. 1989, p. 774–786.
[20] W. C. Jakes, "An approximate method to estimate an upper bound on the effect of multipath delay distortion on digital communications," *IEEE Trans. Commun.*, vol. 27, pp. 76–81, Jan. 1975.

Charles Henry Bianchi was born in Haverhill, MA, on January 4, 1961. He received the B.S., M.S., and Ph.D. degrees in electrical engineering from the University of New Hampshire, Durham, in 1983, 1985, and 1995, respectively.

From 1986 to 1996, he was employed at AT&T Bell Laboratories, North Andover, MA, where he worked on digital radio and hybrid fiber-coax systems. He is currently employed at Sanders Lockheed-Martin in Nashua, NH, where he is working on wireless and hybrid-fiber coax systems. His fields of research activity include RF propagation and planning, as well as channel measurement, characterization, and modeling.

Kondagunta Sivaprasad was born in Madras, India, on March 3, 1935. He received the B.E. degree from the University of Madras, in 1956, and the S.M. and Ph.D. degrees from Harvard University, Cambridge, MA, in applied physics, in 1958 and 1963, respectively.

Since 1969, he has been a member of the Electrical Engineering Department at the University of New Hampshire, Durham. Prior to that, he taught at the Indian Institute of Technology, Madras, India, and at the University of Houston, TX. He also worked at the Air Force Labs at Hanscom Field, Bedford, MA. He was a Visiting Professor at the Technical University of Denmark, Lyngby, in 1976, a Visiting Scientist at Woods Hole Oceanographic Institute, Falmouth, MA, from 1983 to 1984, and a Postdoctoral AFOSR Research Fellow at Rome Labs, Hanscom AFB, from 1990 to 1993. His fields of research activity include applied electromagnetics, wave propagation in inhomogeneous media, underwater acoustics, and remote sensing.